Article

Inner nuclear membrane protein TMEM201 maintains endothelial cell migration and angiogenesis by interacting with the LINC complex

Yutian Zhang[1,2,†], Ya Kong[1,2,†], Haoran Guo[1,2], Yun Liu[3], Yi Zang[1,2,4,*], and Jia Li[1,2,3,4,5,*]

[1] University of Chinese Academy of Sciences, Beijing 100049, China
[2] State Key Laboratory of Drug Research, Shanghai Institute of Materia Medica, Chinese Academy of Sciences, Shanghai 201203, China
[3] State Key Laboratory of Natural Medicines, Jiangsu Key Laboratory of Drug Screening, China Pharmaceutical University, Nanjing 210009, China
[4] School of Pharmaceutical Science and Technology, Hangzhou Institute for Advanced Study, University of Chinese Academy of Sciences, Hangzhou 310024, China
[5] Open Studio for Druggability Research of Marine Natural Products, Pilot National Laboratory for Marine Science and Technology (Qingdao), Qingdao 266237, China
[†] These authors contributed equally to this work.
* Correspondence to: Yi Zang, E-mail: yzang@simm.ac.cn; Jia Li, E-mail: jli@simm.ac.cn

Edited by Xuebiao Yao

The nuclear envelope comprises the outer nuclear membrane, inner nuclear membrane (INM), and nucleopore. Although ∼60 INM proteins have been identified, only a few of them have been well characterized, revealing their crucial roles. Our group focused on the INM protein transmembrane protein 201 (TMEM201), whose role in cellular function remains to be defined. In this study, we investigated the role of TMEM201 in endothelial cell migration and angiogenesis. Depletion of TMEM201 expression by short hairpin RNA-mediated interference impeded human umbilical vein endothelial cell (HUVEC) angiogenic behavior in tube formation and fibrin gel bead sprouting assays. Meanwhile, TMEM201-deficient HUVECs exhibited impaired migration ability. We next explored the underlying mechanism and found that the N-terminal of TMEM201 interacted with the linker of nucleoskeleton and cytoskeleton complex and was required for regulating endothelial cell migration and angiogenesis. These *in vitro* findings were further confirmed by using *in vivo* models. In *Tmem201*-knockout mice, retinal vessel development was arrested and aortic ring sprouting was defective. In addition, loss of *tmem201* impaired zebrafish intersegmental vessel development. In summary, TMEM201 was shown to regulate endothelial cell migration and control the process of angiogenesis. This study is the first to reveal the role of INM proteins in the vascular system and angiogenesis.

Introduction

The nuclear envelope (NE) is a two-lipid-bilayer barrier that separates the nucleoplasm from the cytoplasm. In addition to nuclear pore complex proteins, other integral membrane proteins reside in the outer nuclear membrane (ONM) and inner nuclear membrane (INM) (Schirmer and Gerace, 2005). The ONM

is continuous with the endoplasmic reticulum, while the INM is distinct and enriched with unique proteins. Although ∼60 INM proteins have been identified in proteomic studies (Dreger et al., 2001; Schirmer et al., 2003), only a handful of INM proteins, such as Emerin, MAN1, LaminB receptor, Sad1p/UNC-84 (SUN), and lamina-associated polypeptides, have been well characterized. Studies of these proteins have revealed crucial roles for INM proteins in the nuclear architecture, chromosome organization, DNA repair, transcriptional control, and so on (Holmer and Worman, 2001; Heessen and Fornerod, 2007; Mekhail and Moazed, 2010; Pawar and Kutay, 2021). However, the functions of many other INM proteins remain unclear.

Our group focused on a novel INM protein with few functional studies encoded by the transmembrane protein 201

(TMEM201) gene (Gene ID: 199953). The human homolog is a 666-amino acid protein with five predicted transmembrane segments (TMSs) (Supplementary Figure S1A). Fluorescent micrographs of ectopic TMEM201-flag confirmed the nuclear membrane location of TMEM201 (Supplementary Figure S1B). The phylogenetic tree shows that TMEM201 is highly conserved throughout metazoans and down to *Danio rerio* (Supplementary Figure S2A) and is widely expressed in different tissues and cells (Fagerberg et al., 2014; Supplementary Figure S2B). These data suggest that TMEM201 is a conserved INM protein, whereas its role in cellular functions remains to be defined.

Angiogenesis is a critical process that occurs during development and is also activated in wound healing. Reconstructing vascular networks is a complex process involving multiple processes and various kinds of cells. Angiogenesis is regulated by a tight balance between pro- and antiangiogenic agents. Quiescent endothelial cells (ECs) rapidly switch to a highly migratory and proliferative state when activated by chemotactic, haptotactic, or mechanotactic stimuli (Lamalice et al., 2007). A subset of the population of ECs (tip cells) sprouts and migrates toward guidance cues, while the other population of ECs (stalk cells) trails behind tip cells and proliferates to elongate the sprouts (Jakobsson et al., 2010).

Our group recently showed that TMEM201 is a positive modulator that regulates the invasion and migration of breast cancer cells (Kong et al., 2022). In addition to tumor cell migration, the process of angiogenesis is also essential for tumor development. Angiogenesis involves a cascade of events, among which EC migration is an essential component. A variant of TMEM201, Samp1, has also been identified to positively regulate nuclear movement during fibroblast polarization and migration (Borrego-Pinto et al., 2012). Therefore, we hypothesized that TMEM201 participates in EC migration and angiogenesis. In this study, we found that knockdown of TMEM201 impeded EC angiogenic behavior. Meanwhile, EC migration was impaired. Mechanistically, TMEM201 interacts with the linker of nucleoskeleton and cytoskeleton (LINC) complex, which plays an important role in cell migration. The N-terminal domain of TMEM201 is required for its interactions and function. Furthermore, the loss of TMEM201 impaired mouse retina vessel and zebrafish embryo intersegmental vessel (ISV) development.

Results

Knockdown of TMEM201 represses EC angiogenic behavior

To examine TMEM201 function in EC angiogenic behavior, short hairpin RNA (shRNA)-mediated gene silencing was applied. We designed two pairs of shRNAs specifically targeting different regions of TMEM201 mRNA (Figure 1A). We assessed the level of TMEM201 silencing by immunoblotting and reverse transcription–quantitative real-time polymerase chain reaction (RT–qPCR). Both TMEM201-shRNA-1# (sh-1#) and TMEM201-shRNA-2# (sh-2#) were verified to successfully knock down TMEM201 in human umbilical vein endothelial cells (HUVECs) (Figure 1B).

TMEM201 knockdown produced a striking failure of HUVEC tube formation, with >50% fewer junctions and branches (Figure 1C and D) compared with the control (scramble) group. Meanwhile, the effect of TMEM201 knockdown on EC sprouting was assessed by a fibrin gel bead sprouting assay. The endothelial cell line EA.hy926 was used. The number and length of EC sprouts decreased significantly after the loss of TMEM201 (Figure 1E and F). In a competitive sprouting assay, differentially labelled ECs (mCherry-scramble-expressed and GFP-sh-1#-expressed ECs) were mixed in a 1:1 ratio (Figure 1G). We found that there were more mCherry-scramble-expressing EC sprouts than GFP-sh-1#-expressing EC sprouts at Day 2 and Day 4 (Figure 1I). To exclude any effect of the fluorescence tag, we performed another competitive sprouting assay with GFP-scramble-expressing and mCherry-sh-1#-expressing ECs (Figure 1H). A similar phenomenon was observed (Figure 1J). These results indicate that TMEM201 expression is positively correlated with EC sprouting ability.

Loss of TMEM201 impedes EC migration and polarity

EC angiogenic behavior involves a cascade of events, among which EC migration is an essential process. To investigate the regulatory effect of TMEM201 on EC migration, a transwell assay was performed. Fewer TMEM201-knockdown (sh-1# and sh-2#) HUVECs migrated to the bottom chambers of the transwells compared with the control (scramble) groups (Figure 2A and B).

The HUVEC proliferation rate was slightly inhibited by TMEM201 knockdown (Supplementary Figure S3). Therefore, a wound healing assay was applied for a shorter test time to eliminate the influence of proliferation. At 8 h after scratching, control HUVECs quickly migrated into the wound, exhibiting an almost 70% wound closure ratio, while the wound healing percentage of TMEM201-knockdown HUVECs was <40% (Figure 2C and D).

A wound healing assay is not only able to evaluate the migration speed of cells when they close the wound, but can also be used to evaluate the behavior of cells after physical injury of a cell layer. In most migrating cells, the nucleus is placed away from the leading edge during polarization to prepare for directional migration, and this can be the rate-limiting step of cell migration (Gomes et al., 2005; Calero-Cuenca et al., 2018). With the help of actin cytoskeletal staining, it was observed that the nucleus of control HUVECs moved away from the wound leading edge, whereas the nuclear positions in TMEM201-knockdown HUVECs were disorganized and random (Figure 2E and F).

We also assessed the orientation of the Golgi apparatus in leading cells to analyze HUVEC polarity. After scratching, we found that the Golgi apparatus reorientation ratio was reduced to 24.1% and 23.3% in TMEM201-deficient HUVECs compared with control HUVECs (45.6%) (Supplementary Figure S4). These results indicate that TMEM201 is crucial for establishing endothelial polarity in cell directional migration.

Chemotaxis is an EC migration mechanism that is driven by growth factors such as vascular endothelial growth factor (VEGF)
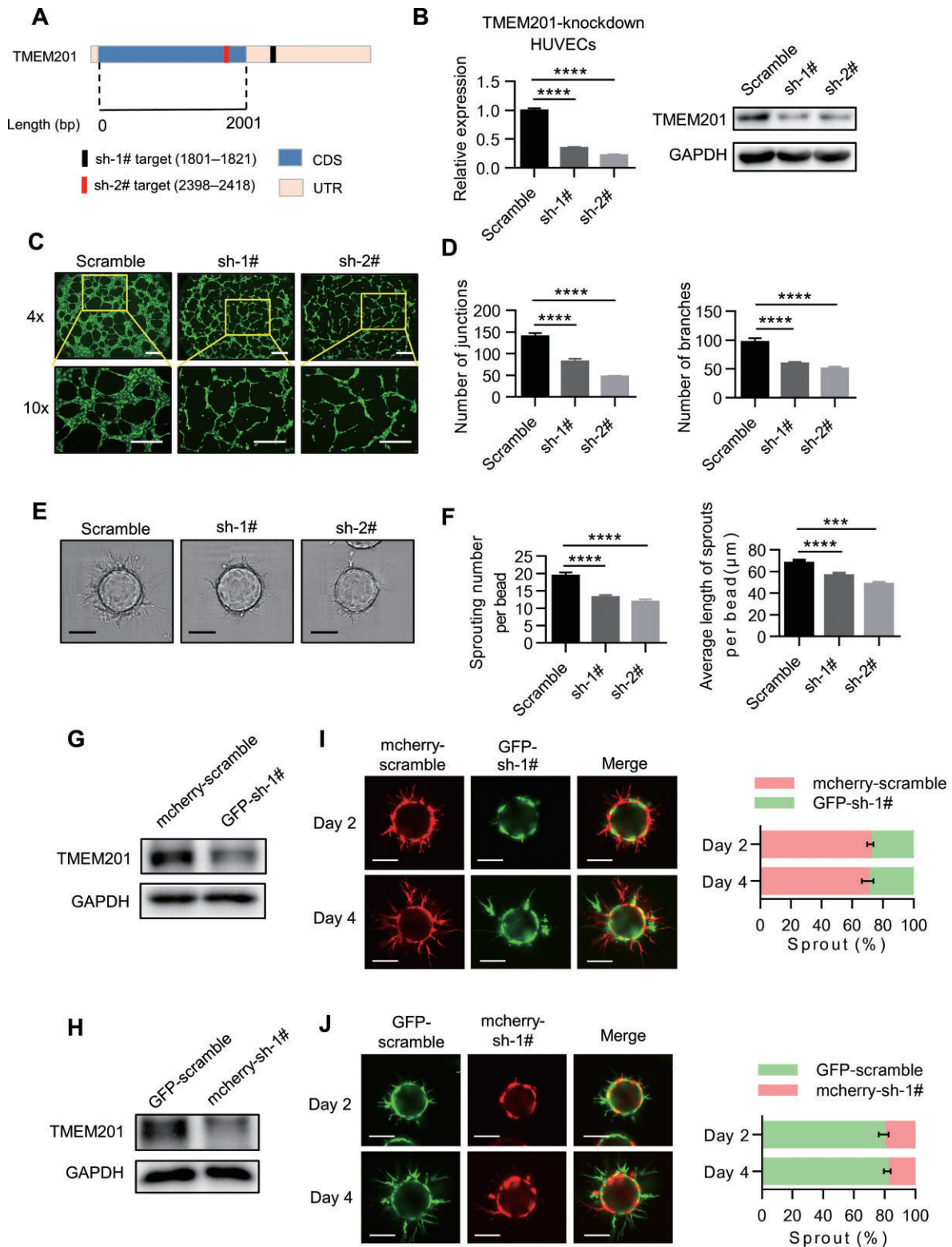
Figure 1 Loss of TMEM201 represses EC tube formation and sprouting capacity. (**A**) The strategy of TMEM201 knockdown. Schematic illustration of TMEM201 mRNA with untranslated regions (UTRs) and coding DNA sequences (CDSs). The positions of the sh-1# and sh-2# targets are indicated. (**B**) RT–qPCR and western blotting analyses show the relative TMEM201 levels in HUVECs expressing control (scramble) or TMEM201 knockdown (sh-1# and sh-2#) shRNA. (**C** and **D**) Knockdown of TMEM201 decreased HUVEC tube formation capacity. (**C**) Representative fluorescent images of the tube formation assay. Tubes were visualized with calcein AM (green), and images were captured at 4× and 10× magnification. Scale bar, 200 μm. (**D**) Quantitative analyses of tube formation. At least six random fields were analyzed for
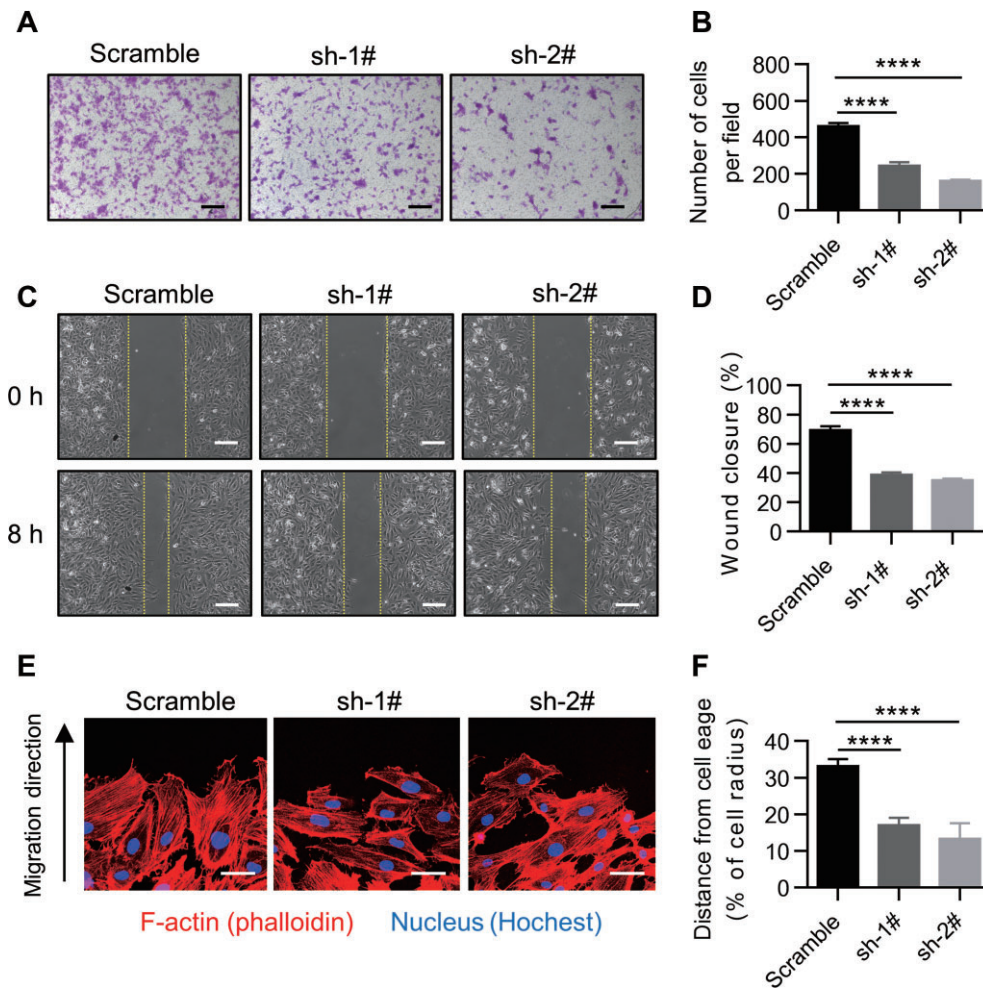
Figure 2 Knockdown of TMEM201 impairs EC migration. (**A** and **B**) The effect of TMEM201 silencing in HUVECs was examined using a transwell assay. (**A**) Representative images of the transwell assay are shown. Scale bar, 200 μm. (**B**) The numbers of migrating cells per field were counted. (**C** and **D**) The effect of TMEM201 silencing in HUVECs was examined using a wound healing assay. (**C**) Representative images at 0 and 8 h after scratching are shown. Yellow dotted lines indicate the migration leading edges. Scale bar, 100 μm. (**D**) The percentage of wound closure was determined at 8 h. (**E**) Representative images of HUVECs at the leading edge in the wound healing assay. Merged images of F-actin (red) and nuclei (blue) are shown. Scale bar, 40 μm. (**F**) Quantitative analysis of nuclear position. The distances away from the leading edge were calculated. Data are presented as mean ± SEM (error bars). Statistical significance was determined by one-way ANOVA (****$P < 0.0001$).

and basic fibroblast growth factor (bFGF) ([Barkefors et al., 2008](#)). However, TMEM201 deficiency did not affect VEGF signaling (Supplementary Figure S5). We suggest that there is another mechanism involved in TMEM201-mediated regulation of EC migration.

TMEM201 interacts with the LINC complex in ECs

The INM localization of TMEM201 limits the pathways in which it may be involved. TMEM201 is likely to regulate cell migration by interacting with proteins localized in the NE or nuclear periphery. The LINC complex is formed by a transluminal

Figure 1 *(Continued)* each group. The number of junctions and branches was quantified with ImageJ. (**E**) Representative images of sprouts at culture Day 4 in control or TMEM201-knockdown EA.hy926 cells. Scale bar, 100 μm. (**F**) Quantification analyses of sprouting. The sprouting number per bead and the average length of sprouts per bead were quantified. (**G**) Western blotting analysis shows TMEM201 levels in EA.hy926 cells expressing mCherry-scramble or GFP-sh-1#. (**H**) Western blotting analysis shows TMEM201 levels in EA.hy926 cells expressing GFP-scramble or mCherry-sh-1#. (**I** and **J**) Competitive sprouting assay with a 1:1 mixture of differentially labelled EA.hy926 cells as indicated. Representative images and quantification of differentially labelled sprouts in each group at culture Day 2 and Day 4 are shown. Scale bar, 100 μm. Data are presented as mean ± SEM (error bars). Statistical significance was determined by one-way ANOVA (***$P < 0.001$, ****$P < 0.0001$).
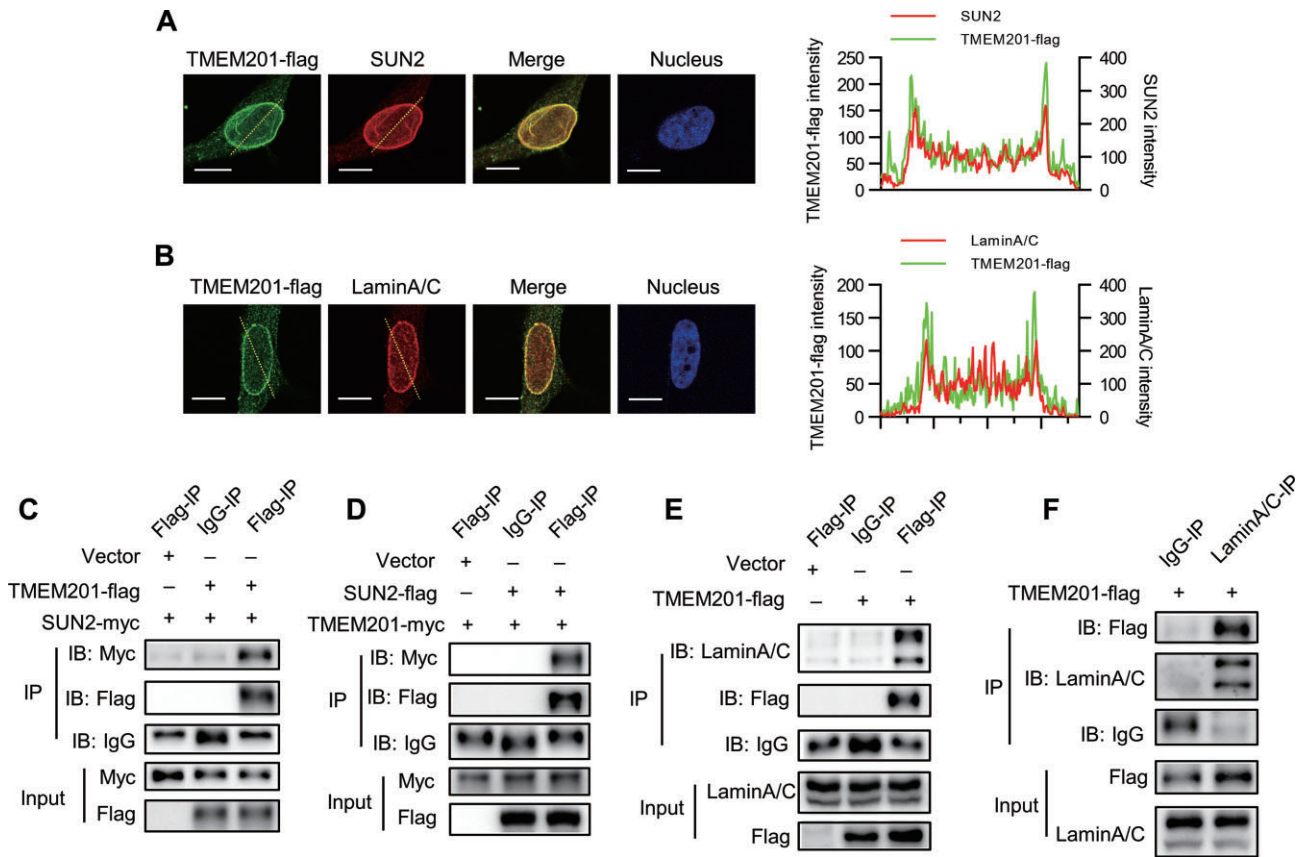
Figure 3 TMEM201 interacts with LINC complex components SUN2 and LaminA/C in EC. (**A** and **B**) TMEM201-flag was detected by immunofluorescence in HUVECs with anti-Flag antibody and costained for SUN2 (**A**) or LaminA/C (**B**). The dotted yellow line was examined for the colocalization analysis, shown on the right. The X-axis shows the relative position of the dotted yellow line. The Y-axis shows the intensity signals in the green and red channels. Scale bar, 10 μm. (**C**) CoIP assay and western blotting analysis show that TMEM201-flag coimmunoprecipitated with SUN2-myc. EA.hy926 cells were transfected with vector or TMEM201-flag together with SUN2-myc. Cell lysates were immunoprecipitated with anti-Flag or control IgG and immunoblotted with antibodies against Flag and Myc. (**D**) CoIP assay and western blotting analysis show that SUN2-flag coimmunoprecipitated with TMEM201-myc. EA.hy926 cells were transfected with vector or SUN2-flag together with TMEM201-myc. Cell lysates were immunoprecipitated with anti-Flag or control IgG and immunoblotted with antibodies against Flag and Myc. (**E**) CoIP assay and western blotting analysis show that TMEM201-flag coimmunoprecipitated with endogenous LaminA/C. EA.hy926 cells were transfected with vector or TMEM201-flag. Cell lysates were immunoprecipitated with anti-Flag or control IgG and immunoblotted with antibodies against Flag and LaminA/C. (**F**) CoIP assay and western blotting analysis show that endogenous LaminA/C coimmunoprecipitated with TMEM201-flag. EA.hy926 cells were transfected with TMEM201-flag. Cell lysates were immunoprecipitated with anti-LaminA/C or control IgG and immunoblotted with antibodies against Flag and LaminA/C.

direct interaction between SUN-domain proteins in the INM and the KASH-domain protein nesprins spanning the ONM. The N-terminus of the SUN protein interacts with lamins or chromatin within the nucleoplasm. The divergent N-terminus of the KASH protein extends into the cytoplasm and engages the cytoskeleton (Alexandre and Misteli, 2010; Supplementary Figure S6). During cell migration, nuclear movement is driven by retrograde actin flow, which depends on actin-associated LINC complexes built of Nesprin-2 giant and SUN2 (Cain et al., 2018).

Whether TMEM201 interacts with the LINC complex was investigated. Because the generated TMEM201 antibody was incapable of immunofluorescence, we expressed ectopic TMEM201-flag for immunofluorescence. Colocalization analysis indicated good potential for a direct interaction between TMEM201

and SUN2 (Figure 3A), as well as LaminA/C (Figure 3B), in ECs. These possible interactions were further confirmed by several coimmunoprecipitation (CoIP) assays. We overexpressed both TMEM201-flag and SUN2-myc. As expected, the immunoblotting data showed that the anti-Flag antibody pulled down SUN2-myc (Figure 3C) and *vice versa* (Figure 3D). Similar assays were performed to test the interaction between TMEM201 and LaminA/C. TMEM201-flag was overexpressed in ECs. After IP with TMEM201-flag, immunoblotting bands for LaminA/C were detected (Figure 3E) and vice versa (Figure 3F). Overall, the immunofluorescence confocal studies and the various CoIP assays verified a specific, direct interaction between TMEM201 and LINC complex components in ECs.

The N-terminus of TMEM201 interacts with the LINC complex and is required for EC migration

According to the predicted TMS and topology with some verification, a schematic diagram of TMEM201 is shown in Figure 4A. TMEM201 has five predicted TMSs. The N-terminus and C-terminus before the last TMS are exposed in the nucleoplasm. To gain further insight into the potential functional relevance of the TMEM201−LINC interaction, we designed a series of Flag-tagged TMEM201 truncations (Figure 4A; Supplementary Figure S7).

First, we found that the TMEM201 N-terminus successfully pulled down SUN2-myc (Figure 4B) and LaminA-myc (Figure 4C), whereas the TMEM201 C-terminus failed to pull down the LINC complex (data not shown). We hypothesized that the N-terminus of TMEM201 is required for LINC complex interaction and EC migration.

Then, the truncation, which lacks the N-terminus (TMEM201△N-flag), was designed for further study. We overexpressed full-length TMEM201-flag or TMEM201△N-flag, together with SUN2-myc or LaminA-myc, followed by CoIP assays. The immunoblotting data showed that full-length TMEM201-flag pulled down the LINC complex, whereas TMEM201△N-flag failed to do so (Figure 4D and E).

In functional assays, full-length TMEM201-flag or TMEM201△N-flag was overexpressed in HUVECs (Figure 4F). We performed transwell, wound healing, and tube formation assays. As expected, expressing full-length TMEM201-flag could accelerate HUVEC migration and angiogenesis. However, expressing TMEM201△N-flag failed to promote migration and angiogenesis (Figure 4G−I). These results indicate that the N-terminus of TMEM201 is necessary and required for TMEM201−LINC complex interaction and the regulation of EC behaviors.

Defective angiogenesis in Tmem201-knockout mice and zebrafish

To further address TMEM201 function in angiogenesis, *Tmem201*-knockout mice were generated by CRISPR/Cas9 technology (Figure 5A; Supplementary Figure S8A), and the knockout efficiency was confirmed (Figure 5B; Supplementary Figure S8B). The *Tmem201*−/− mice were viable.

The mouse retina superficial vascular plexus originates at birth from the optic nerve and grows radially to the peripheral retinal margin during the first postnatal week (Stahl et al., 2010). As a flat and easily imaged plexus, the superficial vascular plexus of newborn mouse retinas is a good model to evaluate gene function in *in vivo* angiogenesis. We found that deletion of *Tmem201* caused a reduction in the extension of the superficial vascular plexus at postnatal day 6 (P6), as measured by radial vascular growth and vascular coverage (Figure 5C).

The aortic ring assay is another angiogenesis model based on organ culture. Mouse aortic rings were prepared using tissues from *Tmem201*+/+ and *Tmem201*−/− mice. As expected, vessel outgrowth and branching from aortic rings

were significantly impaired in the absence of *Tmem201* (Figure 5D).

Vascular development in zebrafish is remarkably similar to that in mice and humans (Staton et al., 2009; Nowak-Sliwinska et al., 2018). The zebrafish homologous *tmem201* gene encodes a 651-amino acid protein. Therefore, a zebrafish embryo model was used to further address the proangiogenic role of TMEM201. We generated *tmem201* deletion mutant zebrafish via CRISPR/Cas9 technology (Figure 5E), and the knockout efficiency was confirmed (Figure 5F).

tmem201+/+ and *tmem201*−/− embryos were collected, and ISV development was evaluated. Embryo ISV sprouts from the aorta, runs between each pair of somites, and connects to the dorsal longitudinal anastomotic vessel (DLAV) at ∼30 h post-fertilization (hpf) (Childs et al., 2002; Tobia et al., 2015). We observed 362 *tmem201*+/+ embryos and 555 *tmem201*−/− embryos in four independent experiments. There was a higher proportion of embryos with defective ISV in *tmem201*−/− embryos (44.5% ± 6.8%) than in *tmem201*+/+ embryos (4.3% ± 2.2%) (Figure 5G). ISV fully extended and had started to form DLAV in *tmem201*+/+ embryos. In *tmem201*−/− embryos, ISV had not fully grown up to the myoseptum, and DLAV was absent (Figure 5H and I).

We microinjected DsRed (control) RNA, tmem201 (rescue) mRNA, tmem201△N-terminus (truncation lacking N-terminus), or tmem201△C-terminus (truncation lacking C-terminus) into fertilized eggs of *tmem201*−/− Tg(fli:EGFP) zebrafish, followed by evaluating embryo vessel development at 30 hpf under a fluorescence microscope. There was a lower proportion of embryos with defective ISV in the rescue group (27.7%) than in the knockout group (44.4%), while tmem201△N-terminus (43.8%) was unable to rescue the phenotype. In addition, tmem201△C-terminus also decreased the ratio of embryos with defective vessels to 24.8% (Supplementary Figure S9). All of these results show that TMEM201 N-terminus is required for vessel development and angiogenesis in zebrafish.

Discussion

In eukaryotic cells, the NE serves as a physical barrier between the nucleus and cytoplasm. The NE is also involved in nucle-ocytoplasmic transport, gene transcription, cell motility, and so on. These functions are carried out by distinct NE proteins, including ONM proteins, INM proteins, and nuclear pore complexes. TMEM201 is a novel INM protein whose role in cellular function remains to be defined. This study is the first to report an essential role of TMEM201 in EC migration and angiogenesis. Our results suggest that TMEM201 regulates EC migration by interacting with the LINC complex.

The INM localization of TMEM201 limits the pathways that it may be involved in. TMEM201 is likely to regulate cell projections by interacting with proteins localized in the NE or nuclear periphery. The LINC complex is formed by a transluminal direct interaction between SUN-domain proteins in the INM and the KASH-domain protein nesprins spanning the ONM. During cell polarization prior to migration, the LINC
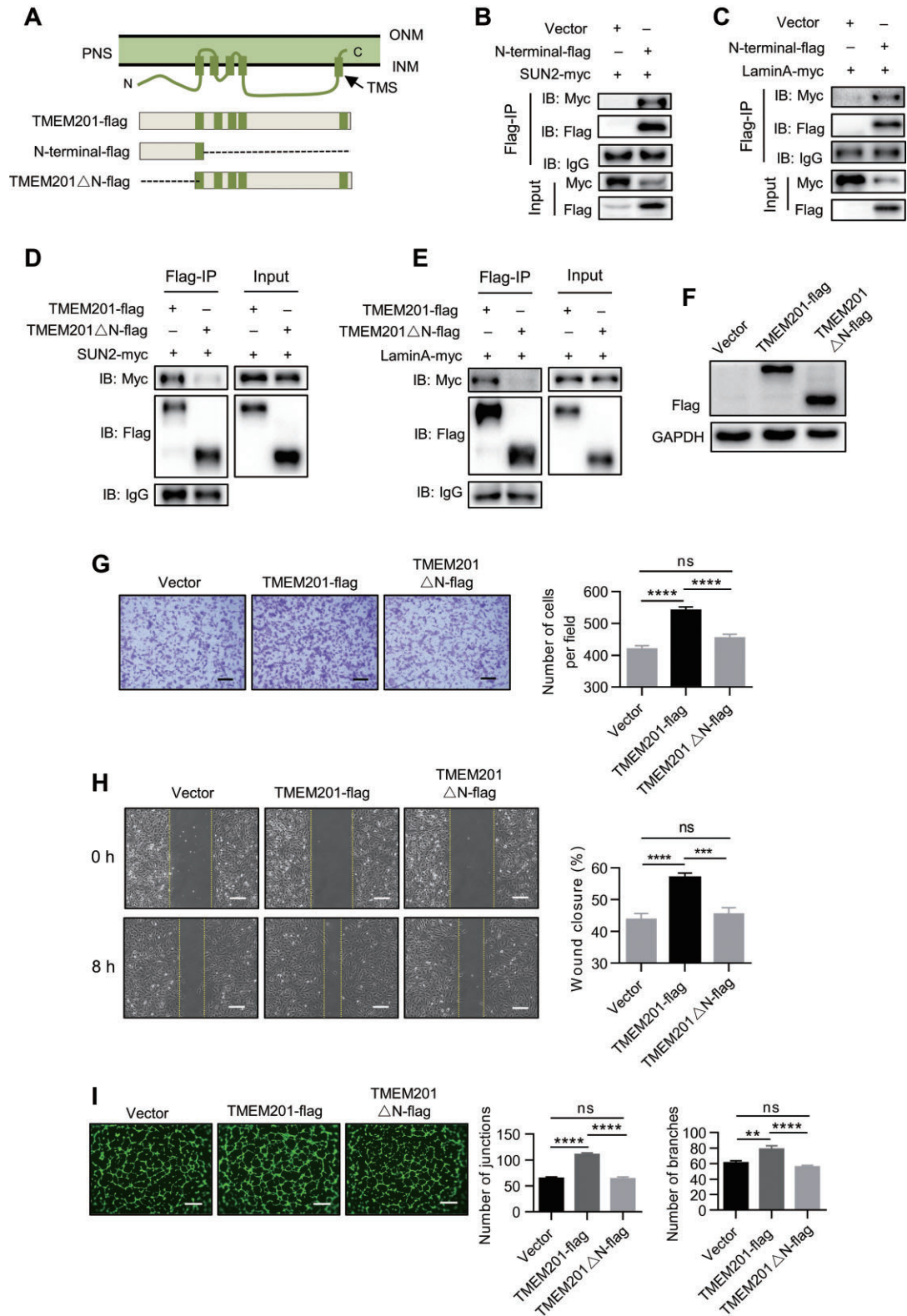
Figure 4 The N-terminus of TMEM201 interacts with the LINC complex and is required for EC migration. (**A**) Schematic diagram of Flag-tagged full-length TMEM201 and several truncations for subsequent experiments. (**B** and **C**) HEK-293T cells were transfected with vector or TMEM201-N-terminal-flag, together with SUN2-myc (**B**) or LaminA-myc (**C**). Cell lysates were immunoprecipitated with anti-Flag and immunoblotted with antibodies against Flag and Myc. (**D** and **E**) HEK-293T cells were transfected with full-length TMEM201-flag or TMEM201△N-flag, together with SUN2-myc (**D**) or LaminA-myc (**E**). Cell lysates were immunoprecipitated with anti-Flag and immunoblotted with antibodies against

complex binds to the actin cytoskeleton and is organized into linear arrays, known as transmembrane actin-associated nuclear lines, to move the nucleus away from the leading edge (Roux et al., 2009).

The LINC complex is present in nearly all cell types, including ECs. The KASH-domain protein nesprins are the ONM components of the LINC complex. Previous studies have shown that depletion of individual nesprin isoforms results in impaired EC migration and polarity. Nesprin-1 depletion increases the number of focal adhesions and substrate traction while decreasing the speed of EC migration (Anno et al., 2012). In addition to Nesprin-1, Nesprin-2 also plays an important role in EC shape and migration by regulating the nuclear and cytoplasmic architecture (King et al., 2014). Nesprin-3 regulates human aortic EC morphology, organizes the perinuclear cytoskeleton, and is required for attaching the centrosome to the NE (Morgan et al., 2010). Recently, another group utilized dominant negative KASH (DN-KASH) to displace endogenous nesprins and disrupt nuclear–cytoskeletal connections. They found that DN-KASH-expressing cells exhibited impaired cell migration in wound healing and angiogenesis (Denis et al., 2021). Collectively, these reports indicate that an intact LINC complex is important for EC function and homeostasis.

In our study, TMEM201 was found to interact with LINC complex components in ECs. Truncation assays indicated that the N-terminus is necessary and required for the interaction and EC migration. The N-terminus of TMEM201 contains a highly conserved Ima1 N-terminal domain (Lu et al., 2020). There are eight conserved cysteines organized as four CxxC motifs, which are predicted to form two zinc fingers. It was previously proven that INM localization of TMEM201 depends on intact CxxC motifs. In addition, TMEM201 zinc finger mutations specifically affect the distribution of Emerin SUN1, and LaminA/C (Gudise et al., 2011).

Samp1 is a shorter isoform of TMEM201 (Buch et al., 2009; Vijayaraghavan et al., 2018). Because the two isoforms share the same N-terminal domain (Supplementary Figure S10), we suggest that Samp1 has a similar function in EC migration and angiogenesis. We overexpressed Samp1-flag in HUVECs (Supplementary Figure S11A). OE-Samp1-flag HUVECs exhibited better migration and tube formation ability than control HUVECs (Supplementary Figure S11B and C). In contrast to Samp1, TMEM201 has a unique undefined C-terminal domain (Supplementary Figure S10). The nucleocytoplasmic C-terminus of TMEM201 is highly conserved, but its role is poorly understood. Although the C-terminus was not identified to be involved in LINC complex interactions, we suggest that the C-terminal domain may play another specific role. For example, a number of phosphorylation sites have been identified in the TMEM201 C-terminus (Dephoure et al., 2008; Olsen et al., 2010; Zhou et al., 2013; Schaffer et al., 2015), implying a potential regulatory function of the C-terminal domain.

There are several hypotheses about the detailed mechanisms by which TMEM201 regulates SUN2 and LaminA/C. Lamins, the major constituent of the nuclear lamina, form a dense meshwork of filaments. Numerous INM proteins, such as LAP2–Emerin–MAN1-domain proteins, help anchor lamin filaments to the NE (Schirmer and Foisner, 2007; Barton et al., 2015; Leeuw et al., 2018). We suggest that TMEM201 associates with LaminA/C and contributes to tethering lamin filaments around the nuclear periphery. On the other hand, Samp1 was previously reported to significantly attenuate the mobility of another INM protein, Emerin, in the NE (Vijayaraghavan et al., 2018). We suggest that TMEM201 may also serve as an anchor to restrict the mobility of SUN2. As a result, the flexibility and stabilization of the LINC complex might be adjusted to adapt to specific situations.

There are other potential mechanisms by which TMEM201 could impact EC migration independently of its interaction with the LINC complex. Chemotaxis is a mechanism of EC migration and angiogenesis driven by growth factors such as VEGF and bFGF (Barkefors et al., 2008). However, we found that TMEM201 deficiency did not affect VEGF signaling in HUVECs. In addition to the prominent role of VEGF, other signaling pathways, such as Notch and transforming growth factor-β (TGFβ), contribute to angiogenesis through coordinated crosstalk. Whether TMEM201 regulates these pathways remains to be elucidated. Most recently, our group showed that TMEM201 is a positive modulator that regulates the invasion of breast cancer cells. TMEM201 deficiency inhibits epithelial to mesenchymal transition and TGFβ signaling (Kong et al., 2022). Given our findings, it is an attractive possibility that TMEM201 might regulate EC migration and polarity through the TGFβ-dependent signaling pathway.

We applied tube formation and fibrin gel bead sprouting assays to recapitulate *in vivo* angiogenesis. These models provide a setting that is closer to the local environment *in vivo*, where ECs are surrounded by matrix and can form tube-like structures in response to growth factors or other matrix proteins. The results showed that loss of TMEM201 impaired EC tube formation and sprouting ability.

Encouraged by these results, we further investigated TMEM201 function in angiogenesis *in vivo*. *Tmem201*-knockout

---

Figure 4 *(Continued)* Flag and Myc. (**F**) Western blotting analyses show the relative TMEM201 expression in TMEM201-flag- or TMEM201△N-flag-expressing HUVECs. (**G–I**) The effects of full-length TMEM201-flag and TMEM201△N-flag in HUVECs were examined using transwell, wound healing, and tube formation assays. (**G**) Representative images of the transwell assay are shown. Scale bar, 200 μm. The numbers of migrating cells per field were counted. (**H**) Representative images at 0 and 8 h after scratching are shown. Yellow dotted lines indicate the migration leading edges. The percentage of wound closure was determined at 8 h. Scale bar, 100 μm. (**I**) Representative fluorescent images and quantitative analyses of the tube formation assay. Tubes were visualized with calcein AM (Green). Scale bar, 200 μm. Data are presented as mean ± SEM (error bars). Statistical significance was determined by one-way ANOVA (**$P < 0.01$, ***$P < 0.001$, ****$P < 0.0001$, and ns = no significance).
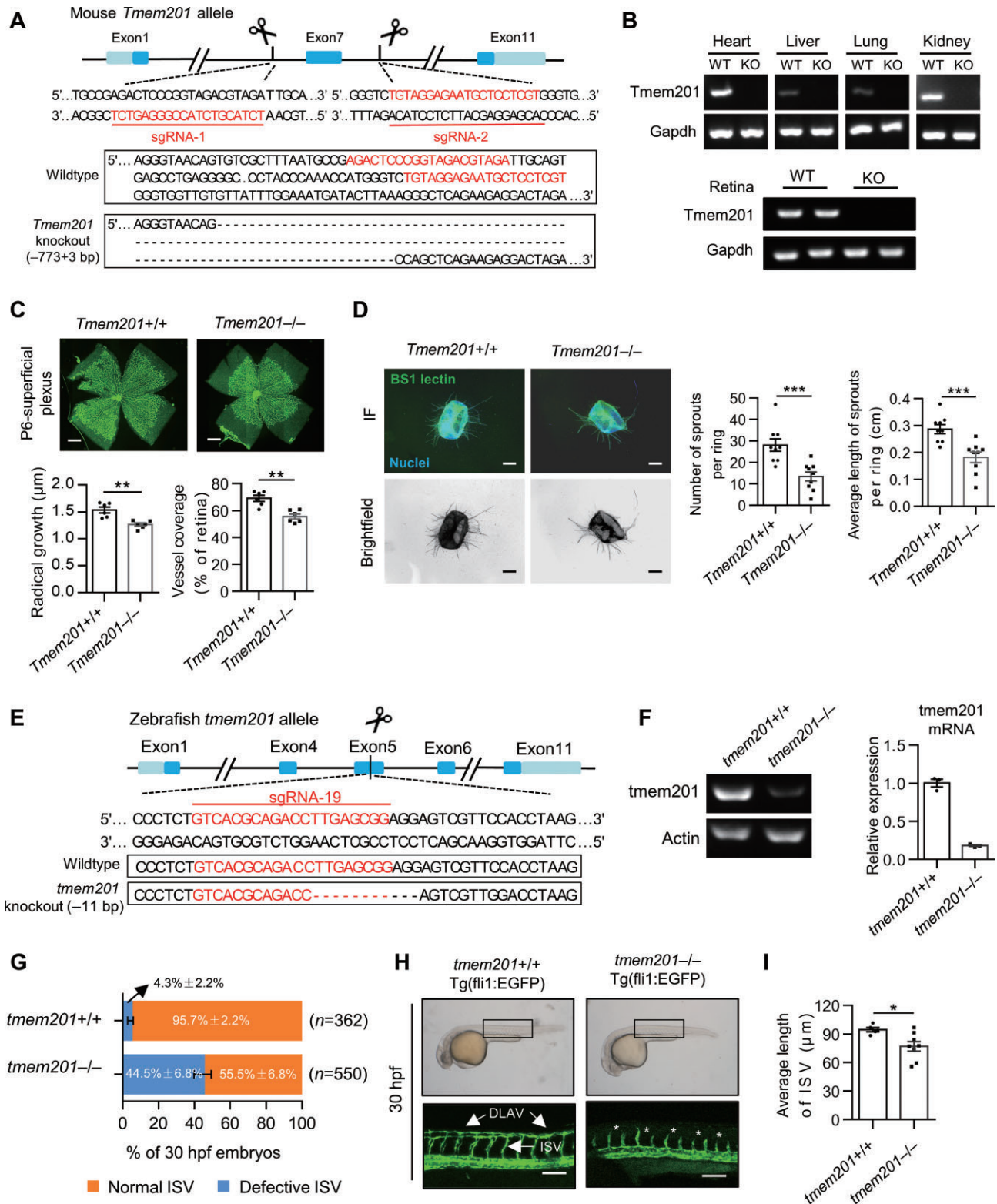
Figure 5 Defective angiogenesis in *Tmem201*-knockout mice and *tmem201*-knockout zebrafish. (**A**) Schematic diagram of CRISPR/Cas9-mediated knockout of the mouse *Tmem201* allele. The sequences of sgRNAs and corresponding deletion sites are shown. (**B**) RT–PCR for *Tmem201* and *Gapdh* performed on mRNA extracted from tissues of the indicated mice. (**C**) Representative images of whole-mounted retinas from *Tmem201*+/+ and *Tmem201*−/− mice at P6. Retinal vessels were stained with Isolectin GS-IB4 (green). Scale bar, 500 μm. Reduced extension of the superficial plexus was quantitated in the retina of *Tmem201*+/+ and *Tmem201*−/− mice (*n* = 6 for each group). (**D**) Aortic ring assays of *Tmem201*+/+ and *Tmem201*−/− mice. EC sprouts were stained with BSI lectin (green). Scale bar, 200 μm. The number of

mice were viable but exhibited a delay in the development of the superficial vascular plexus at P6. From P7 to P15, the superficial capillaries sprout vertically to form the deep vascular plexus, followed by the formation of an intermediate vascular plexus from P15 to P21 (Stahl et al., 2010). We tested other retinal vessel development stages. At P9, *Tmem201+/+* and *Tmem201−/−* mice had comparable vessel coverage in the superficial plexus, while the deep plexus of *Tmem201−/−* mice grew slower than that of *Tmem201+/+* mice (Supplementary Figure S12). At P17, the retinal vessel development of *Tmem201−/−* mice was similar to that of *Tmem201+/+* mice (Supplementary Figure S13). It seems that *Tmem201−/−* mice exhibited a delay in the development of the superficial vascular plexus at P6 and deep vascular plexus at P9, whereas vessel development at P17 was resolved. It remains to be explored whether the delay of retinal vessel development causes any retinopathy or visual defects in *Tmem201*-knockout mice (Selvam et al., 2018).

In zebrafish, we tested embryo vessel development at 54 hpf and 5 days postfertilization (dpf). A lower proportion of embryos with normal vessels were observed in the *tmem201*-deficient group (66.3% ± 10.7% at 54 hpf and 79.6% ± 7.6% at 5 dpf) than in the control group (95.7% ± 2.2%) (Supplementary Figure S14). The formation of new blood vessels, or angiogenesis, is a complex process that plays important roles in growth and development, tissue and organ regeneration, and numerous pathological conditions. In our study, TMEM201 was found to play an important role during mouse retina and zebrafish ISV development (also known as physiological angiogenesis). Of course, TMEM201's function in pathological angiogenesis remains to be elucidated. The two most prominent pathological angiogenesis models are retinopathy pathological angiogenesis (Liu et al., 2017; Selvam et al., 2018) and tumor angiogenesis (Maishi and Hida, 2017; Lugano et al., 2020). Oxygen-induced retinopathy (Connor et al., 2009) and choroidal neovascularization models (Toma et al., 2010; Shah et al., 2015) will be utilized in future studies.

Materials and methods
Cell lines and cell culture

Primary HUVECs (Promocell, C-12203) were cultured in endothelial cell growth medium 2 (EGM2) with a supplemental mix (Promocell, C-22011) and were used at passages 3–8. EA.hy926 (ATCC, CRL-2922), HEK-293T (Clontech, 632180), and NIH-3T3 (ATCC, CRL-1658) cells were cultured in Dulbecco's modified Eagle's medium supplemented with 10% fetal bovine serum

(FBS). All cells were maintained in a humidified atmosphere at 37°C and 5% CO_2.

Generation of TMEM201-knockdown or TMEM201-overexpressing ECs

shRNA was designed with BLOCK-iT™ RNA Designer (Invitrogen). The shRNA sequences (21 bp sense) are as follows. Scramble: CAACAAGATGAAGAGCACCAA; sh-1#: GCGTAGTCA CATCTTTGTACT; and sh-2#: GCAACCGCTCCATCAAGAAAG. shRNA was cloned into the pLKO.1 plasmid following the protocol from Addgene (Moffat et al., 2006). shRNA plasmid, psPAX2, and pMD2.G (4:3:1) were cotransfected into HEK-293T cells using Lipofectamine 2000 (Thermo Fisher Scientific, 11668019). After 48 h, the supernatant was collected and filtered through a 0.45-μm membrane (Millipore) to obtain knockdown virus particles. Human TMEM201, LaminA, and SUN2 cDNAs were cloned into the pLVX-IRES plasmid with a Flag or Myc tag. The overexpression plasmids psPAX2 and VSVG (5:3:2) were cotransfected into HEK-293T cells, and overexpression virus particles were collected. HUVECs or EA.hy926 cells were infected with the appropriate amount of knockdown or overexpression virus particles. After 48 h, the infected ECs were subjected to various tests.

Tube formation assay

Tube formation assay was based on a published protocol (Arnaoutova and Kleinman, 2010). A 96-well plate was coated with 50 μl Cultrex Basement Membrane Extract (Trevigen, 3433-010-01) and incubated at 37°C for 30 min. HUVECs (1.2×10^4) were seeded in the wells. After 4–6 h of incubation, the tubes were stained with calcein AM. Brightfield and fluorescent images were taken from several fields. The brightfield images were analyzed using the 'Angiogenesis Analyzer' plugin in ImageJ.

Fibrin gel bead sprouting assay

A previously established fibrin gel bead sprouting assay was optimized to study angiogenesis (Nakatsu et al., 2007; Nakatsu and Hughes, 2008). A total of 2500 Cytodex microcarrier beads (Sigma-Aldrich, C3275) were coated with 1×10^6 EA.hy926 in medium at 37°C and 5% CO_2. The tube was shaken gently every 20 min for 4 h. The coated beads were then transferred to a dish containing 5 ml EGM2 medium and left overnight. The next day, the EA.hy926-coated beads were resuspended at a concentration of 500 beads/ml in 2 mg/ml fibrinogen (Sigma-Aldrich, F3879) solution containing 0.15 U/ml aprotinin

Figure 5 *(Continued)* sprouts and the average length of sprouts emerging from the aortic ring were determined. (**E**) Schematic diagram of CRISPR/Cas9-mediated knockout of the zebrafish *tmem201* allele. The sequence of sgRNA and its corresponding deletion sites are shown. (**F**) RT–PCR and qPCR for *tmem201* and *actin* performed on mRNA extracted from the tissue of the indicated zebrafish. (**G**) The percentages of 30-hpf *tmem201+/+* and *tmem201−/−* embryos with normal or defective ISV. Four independent trials were performed, and the numbers of embryos are shown. (**H**) Representative images of 30-hpf embryos. In *tmem201+/+* embryos, ISV fully extended and started to form DLAV. In *tmem201−/−* embryos, ISV did not extend completely, and DLAV was absent. ISV and DLAV are indicated with white arrows. White asterisks represent defective ISV. Scale bar, 500 μm. (**I**) Quantitative analyses of embryo ISV development in **H**. The average length of ISV was calculated for each group (*n* = 5 for *tmem201+/+* and *n* = 8 for *tmem201−/−*). Data are presented as mean ± SEM (error bars). Statistical significance was determined by Student's *t*-test (**P* < 0.05, ***P* < 0.01, ****P* < 0.001).

(Meilunbio, MB3095). Then, 0.625 U/ml thrombin (Meilunbio, MB1368) was added to a 24-well plate, followed by the addition of the fibrinogen/bead solution. The plate was left at room temperature for 5 min and then placed in an incubator at 37°C and 5% CO_2 for 15 min to generate a clot. Finally, fibroblast NIH-3T3 cells were seeded on top of the fibrin gel at a concentration of 2×10^4 cells/well in 1 ml EGM2 medium. The medium was changed every other day. Sprouting images were captured after 2–4 days.

Transwell assay

HUVECs were loaded onto 8-μm-pore-size transwell chambers (Corning, CLS3422) in 100 μl EGM2 medium at a concentration of 5×10^4 cells/well. Medium with 10% FBS was added to the lower well. After 24 h, the cells were fixed and stained with 0.1% crystal violet. Non-migrating cells on the upper surface of the chamber were removed by wiping with a cotton swab. Images were captured by microscopy, and the migrating cell number was counted using ImageJ.

Wound healing assay

A wound healing assay was conducted using a Culture-Insert 3 Well Dish (Ibidi, 80366). HUVECs were seeded at a concentration of 3×10^5 cells/ml and incubated overnight. After removing the insert, fresh medium was added. Images of the gap at the indicated time points were collected at the same magnification. The degree of wound healing was determined by quantification of the wound area at the time points compared with that at 0 h.

Cell viability assay

Cell viability was detected by Cell Counting Kit-8 (CCK8) according to the manufacturer's guidelines. Ten microliters of CCK8 (Dojindo, CK04) solution was added to each well containing 90 μl culture medium, followed by gentle shaking. After incubation at 37°C under 5% CO_2 for 1–4 h, the absorbance of the solutions was measured at 450 nm using an M5 microplate reader (Molecular Device).

Immunofluorescence

Cells were fixed with 4% paraformaldehyde solution, permeabilized with 0.2% Triton X-100 solution, blocked with 5% bovine serum album solution, and then incubated with primary antibody at 4°C overnight. The samples were washed and treated with fluorescent secondary antibody at room temperature for 1 h. For F-actin staining, the samples were incubated with phalloidin (1:100) for 1 h. The nuclei were stained with Hoechst 33342 (1:2000). The samples were imaged with a Leica SP5 confocal microscope. Colocalization analyses were performed by ImageJ.

RT–qPCR

Total RNA from cultured cells and animal tissues was extracted using TRIzol according to the manufacturer's instructions. cDNA was synthesized with ABScript II RT Master Mix

(ABclonal, RK20402), and qPCR was performed using 2× Universal SYBR Green Fast qPCR Mix (ABclonal, RM21203) following the manufacturer's instructions. The following primers were used: human TMEM201 forward 5′-AGCAACCGCTCCATCAAGAA-3′ and reverse 5′-CGCAGGCTCTGGTACAGAAA-3′, human GAPDH forward 5′-AAGAAGGTGGTGAAGCAGG-3′, and reverse 5′-AGGTGGAGGAGTGGGTGTCG-3′, mouse Tmem201 forward 5′-CAAGTGTCACATCCTCGCCA-3′, and reverse 5′-CTCCCGCTGAACAGGTATCC-3′, mouse Gapdh forward 5′-AGGTCGGTGTGAACGGATTTG-3′ and reverse 5′-TGTAGACCATGTAGTTGAGGTCA-3′, zebrafish tmem201 forward 5′-CTCGCCACCTTCAGACTACT-3′ and reverse 5′-TCTGAAAGAAACGGAGGCGG-3′, and zebrafish actin forward 5′-ATGCCCCTCGTGCTGTTTTC-3′ and reverse 5′-GCCTCATCTCCCACATAGGA-3′. The level of target gene expression was normalized to that of GAPDH or actin.

CoIP and immunoblotting

First, 400 μl of diluted antibody (Ab) was added to Protein A/G Magnetic Beads (MedChemExpress, HY-K0202), and the tube was rotated for 2 h at 4°C. Then, the bead–Ab complex was washed five times using wash buffer (phosphate-buffered saline with 0.5% Triton X-100, PBST). Cells were lysed with lysis buffer (Beyotime Biotechnology, P0013B) supplemented with protease inhibitor cocktails and incubated for 10 min. After centrifugation, the lysate supernatant was collected. The bead–Ab complex was added to the cell lysate to capture the target antigen (Ag). Afterward, the bead–Ab–Ag was washed with PBST. The precipitate was detected by immunoblotting. Samples were separated by sodium dodecyl sulfate–polyacrylamide gel electrophoresis and probed with the indicated antibodies following standard western blotting procedures. The positive protein bands were visualized with electrochemiluminescence.

Generation of Tmem201-knockout mice

Tmem201-knockout mice were generated by the Shanghai Model Organisms Center (China). Genotyping was performed using DNA extracted from the tail tissue by PCR with the following primers: P1 forward 5′-CGGGCAGCTTGGTGGCGGTTTT-3′, P2 reverse 5′-AGGGATGCTGGCGAGGATGTG-3′, P3 forward 5′-GCGGAGTGCCTGGTCTGGGGATAG-3′, and P4 reverse 5′-CTGGGCAGTGAGTGTGATGTGAAA-3′. Knockout of *Tmem201* was confirmed by RT–PCR in different tissues. Age-, sex-, and strain-matched animals were used throughout. Animals were housed in a temperature-controlled room (22°C ± 2°C) with a 12-h light/dark cycle. All animal experiments were approved by the Animal Ethics Committee of the Shanghai Institute of Materia Medica.

Retina isolation and whole-mount staining

The neonatal mouse retina was isolated and subjected to whole-mount staining following a protocol described previously with some modifications (Tual-Chalot et al., 2013). Briefly, the eyes were fixed in methanol overnight at −20°C. After fixation, the retinas were dissected, washed, and permeabilized with 0.5% Triton X-100 overnight at 4°C and then stained with Isolectin GS-IB4 conjugate overnight at 4°C. Finally, the retinas

were transferred onto slides with four radial incisions to create a 'petal' shape and mounted. Images were taken by Vectra (PerkinElmer).

Aortic ring assay

The aortic ring assay was performed using a modified method (Marianne et al., 2011). In brief, 0.5-mm-diameter rings were sliced from the aortas of 8-week-old mice. The aortic rings were embedded into collagen I gel in a 48-well plate and cultured in Opti-MEM supplemented with 2.5% FBS and 30 ng/ml VEGF. The medium was changed every other day. After 6 days of culture, the explants were fixed and stained with BSI lectin-FITC and Hoechst 33342. The aortic rings were visualized under a microscope. The number and length of the branches were counted manually.

Generation of tmem201-knockout zebrafish

tmem201-knockout zebrafish were generated using the CRISPR/Cas9 gene editing system by Xinjia Medical Co. Ltd (China). Briefly, small guide RNA (sgRNA) targeting the zebrafish *tmem201* gene (NC_007134.7) was designed by the online software CHOPCHOP. AB strain zebrafish embryos were microinjected with sgRNA as previously described (Hwang et al., 2013). The efficiency of knockout was estimated by a PCR-based method at 2 days postinjection (Carrington et al., 2015). The most efficient sgRNA was selected for the generation of the mutant line: sgRNA19 5′-GTCACGCAGACCTTGAGCGG-3′. The injected zebrafish (F0) were raised and crossed with the AB strain to obtain the founder. One strain with an allele containing a frameshift deletion resulting in a premature stop codon was selected and crossed with Tg(fli:EGFP) transgenic zebrafish for the angiogenesis experiments. Genotyping was performed using DNA extracted from the adult zebrafish caudal fin by a PCR assay with the following primers: forward 5′-GCAGCTACTGTTGATTCA TG-3′ and reverse 5′-CTGAATTCCAGTACTTCGAC-3′.

ISV phenotype evaluation

Embryos at 30 hpf were collected from different groups, and ISV phenotypes were evaluated. For ISV phenotype quantitation, the phenotypes were divided into two groups: normal ISV (ISV fully extends dorsally) and defective ISV (no ISV sprouts or ISV up to the horizontal myoseptum). In addition, the length of ISV was measured for phenotype quantitation.

Antibodies and materials

The antibodies and fluorescent dyes used in this study were as follows: anti-Flag (FUJIFILM Wako, 018-22381), normal mouse IgG (Santa Cruz, sc-2025), and calcein AM (MB5279, Meilunbio). Anti-GAPDH (14C10) rabbit mAb (2118S), LaminA/C (4C11) mouse mAb (4777S), and Myc-tag (9B11) mouse mAb (2276S) were purchased from Cell Signaling Technology. Anti-SUN2 antibody [EPR6557] (ab124916), goat anti-rabbit IgG H&L (Alexa Fluor® 488) (ab150077), and goat anti-mouse IgG H&L (Alexa Fluor® 555) (ab150114) were purchased from Abcam. Peroxidase AffiniPure goat anti-mouse IgG (H+L) (115-035-003) and peroxidase AffiniPure rabbit anti-goat IgG (H+L) (305-035-003) were purchased from Jackson ImmunoResearch Laboratories.

F-actin monoclonal antibody (NH3) (MA1-80729), Alexa Fluor 488 Isolectin GS-IB4 conjugate (I21411), and Hoechst 33342 solution (H3570) were purchased from Invitrogen. γ-tubulin antibody (T6557) and BSI lectin-FITC (L9381) were purchased from Sigma-Aldrich. The anti-TMEM201 rabbit antibody, generated with the TMEM201 (430–638 amino acid) peptide, was made by Youke Biological Technology Co. Ltd.

Statistical analysis

Data are presented as mean ± standard error of the mean (SEM). The statistical evaluations were analyzed with GraphPad Prism 6 and performed by Student's *t*-test (two-tailed) for comparisons between two groups and one-way analysis of variance (ANOVA) with Bonferroni correction for comparisons between multiple groups. *P*-values are indicated as follows: $*P < 0.05$, $**P < 0.01$, $***P < 0.001$, and $****P < 0.0001$.

Supplementary material

Supplementary material is available at *Journal of Molecular Cell Biology* online.

Conflict of interest: none declared.

References

Alexandre, M.A., and Misteli, T. (2010). LINC complexes in health and disease. Nucleus *1*, 40–52.

Anno, T., Sakamoto, N., and Sato, M. (2012). Role of nesprin-1 in nuclear deformation in endothelial cells under static and uniaxial stretching conditions. Biochem. Biophys. Res. Commun. *424*, 94–99.

Arnaoutova, I., and Kleinman, H.K. (2010). In vitro angiogenesis: endothelial cell tube formation on gelled basement membrane extract. Nat. Protoc. *5*, 628–635.

Barkefors, I., Jan, S.L., Jakobsson, L., et al. (2008). Endothelial cell migration in stable gradients of vascular endothelial growth factor A and fibroblast growth factor 2: effects on chemotaxis and chemokinesis. J. Biol. Chem. *283*, 13905–13912.

Barton, L.J., Soshnev, A.A., and Geyer, P.K. (2015). Networking in the nucleus: a spotlight on LEM-domain proteins. Curr. Opin. Cell Biol. *34*, 1–8.

Borrego-Pinto, J., Jegou, T., Osorio, D.S., et al. (2012). Samp1 is a component of TAN lines and is required for nuclear movement. J. Cell Sci. *125*, 1099–1105.

Buch, C., Lindberg, R., Figueroa, R., et al. (2009). An integral protein of the inner nuclear membrane localizes to the mitotic spindle in mammalian cells. J. Cell Sci. *122*, 2100–2107.

Cain, N.E., Jahed, Z., Schoenhofen, A., et al. (2018). Conserved SUN–KASH interfaces mediate LINC complex-dependent nuclear movement and positioning. Curr. Biol. *28*, 3086–3097.e4.

Calero-Cuenca, F.J., Janota, C.S., and Gomes, E.R. (2018). Dealing with the nucleus during cell migration. Curr. Opin. Cell Biol. *50*, 35–41.

Carrington, B., Varshney, G.K., Burgess, S.M., et al. (2015). CRISPR–STAT: an easy and reliable PCR-based method to evaluate target-specific sgRNA activity. Nucleic Acids Res. *43*, e157.

Childs, S., Chen, J.N., Garrity, D.M., et al. (2002). Patterning of angiogenesis in the zebrafish embryo. Development *129*, 973–982.

Connor, K.M., Krah, N.M., Dennison, R.J., et al. (2009). Quantification of oxygen-induced retinopathy in the mouse: a model of vessel loss, vessel regrowth and pathological angiogenesis. Nat. Protoc. *4*, 1565–1573.

Denis, K.B., Cabe, J.I., Danielsson, B.E., et al. (2021). The LINC complex is required for endothelial cell adhesion and adaptation to shear stress and cyclic stretch. Mol. Biol. Cell *32*, 1654–1663.

Dephoure, N., Zhou, C.S., Villén, J., et al. (2008). A quantitative atlas of mitotic phosphorylation. Proc. Natl Acad. Sci. USA *105*, 10762–10767.

Dreger, M., Bengtsson, L., Schöneberg, T., et al. (2001). Nuclear envelope proteomics: novel integral membrane proteins of the inner nuclear membrane. Proc. Natl Acad. Sci. USA *98*, 11943–11948.

Fagerberg, L., Hallström, B.M., Oksvold, P., et al. (2014). Analysis of the human tissue-specific expression by genome-wide integration of transcriptomics and antibody-based proteomics. Mol. Cell. Proteomics *13*, 397–406.

Gomes, E.R., Jani, S., and Gundersen, G.G. (2005). Nuclear movement regulated by Cdc42, MRCK, myosin, and actin flow establishes MTOC polarization in migrating cells. Cell *121*, 451–463.

Gudise, S., Figueroa, R.A., Lindberg, R., et al. (2011). Samp1 is functionally associated with the LINC complex and A-type lamina networks. J. Cell Sci. *124*, 2077–2085.

Heessen, S., and Fornerod, M. (2007). The inner nuclear envelope as a transcription factor resting place. EMBO Rep. *8*, 914–919.

Holmer, L., and Worman, H.J. (2001). Inner nuclear membrane proteins: functions and targeting. Cell. Mol. Life Sci. *58*, 1741–1747.

Hwang, W.Y., Fu, Y., Reyon, D., et al. (2013). Efficient genome editing in zebrafish using a CRISPR–Cas system. Nat. Biotechnol. *31*, 227–229.

Jakobsson, L., Franco, C.A., Bentley, K., et al. (2010). Endothelial cells dynamically compete for the tip cell position during angiogenic sprouting. Nat. Cell Biol. *12*, 943–953.

King, S.M., Nowak, K., Suryavanshi, N., et al. (2014). Nesprin-1 and nesprin-2 regulate endothelial cell shape and migration. Cytoskeleton *71*, 423–434.

Kong, Y., Zhang, Y.T., Wang, H.L., et al. (2022). Inner nuclear membrane protein TMEM201 promotes breast cancer metastasis by positive regulating TGFβ signaling. Oncogene *41*, 647–656.

Lamalice, L., Boeuf, F.L., and Huot, J. (2007). Endothelial cell migration during angiogenesis. Circ. Res. *100*, 782–794.

Leeuw, R.D., Gruenbaum, Y., and Medalia, O. (2018). Nuclear lamins: thin filaments with major functions. Trends Cell Biol. *28*, 34–45.

Liu, C.H., Wang, Z.X., Sun, Y., et al. (2017). Animal models of ocular angiogenesis: from development to pathologies. FASEB J. *31*, 4665–4681.

Lugano, R., Ramachandran, M., and Dimberg, A. (2020). Tumor angiogenesis: causes, consequences, challenges and opportunities. Cell. Mol. Life Sci. *77*, 1745–1770.

Lu, S., Wang, J.Y., Chitsaz, F., et al. (2020). CDD/SPARCLE: the conserved domain database in 2020. Nucleic Acids Res. *48*, D265–D268.

Maishi, N., and Hida, K. (2017). Tumor endothelial cells accelerate tumor metastasis. Cancer Sci. *108*, 1921–1926.

Marianne, B., Stephen, D.R., Tanguy, L., et al. (2011). Use of the mouse aortic ring assay to study angiogenesis. Nat. Protoc. *7*, 89–104.

Mekhail, K., and Moazed, D. (2010). The nuclear envelope in genome organization, expression and stability. Nat. Rev. Mol. Cell Biol. *11*, 317–328.

Moffat, J., Grueneberg, D.A., Yang, X.P., et al. (2006). A lentiviral RNAi library for human and mouse genes applied to an arrayed viral high-content screen. Cell *124*, 1283–1298.

Morgan, J.T., Pfeiffer, E.R., Thirkill, T.L., et al. (2011). Nesprin-3 regulates endothelial cell morphology, perinuclear cytoskeletal architecture, and flow-induced polarization. Mol. Biol. Cell *22*, 4324–4334.

Nakatsu, M.N., Davis, J., and Hughes, C.C. (2007). Optimized fibrin gel bead assay for the study of angiogenesis. J. Vis. Exp. *3*, 186.

Nakatsu, M.N., and Hughes, C.C. (2008). An optimized three-dimensional in vitro model for the analysis of angiogenesis. Methods Enzymol. *443*, 65–82.

Nowak-Sliwinska, P., Alitalo, K., Allen, E., et al. (2018). Consensus guidelines for the use and interpretation of angiogenesis assays. Angiogenesis *21*, 425–532.

Olsen, J.V., Vermeulen, M., Santamaria, A., et al. (2010). Quantitative phosphoproteomics reveals widespread full phosphorylation site occupancy during mitosis. Sci. Signal. *3*, ra3.

Pawar, S., and Kutay, U. (2021). The diverse cellular functions of inner nuclear membrane proteins. Cold Spring Harb. Perspect. Biol. *13*, a040477.

Roux, K.J., Crisp, M.L., Liu, Q., et al. (2009). Nesprin 4 is an outer nuclear membrane protein that can induce kinesin-mediated cell polarization. Proc. Natl Acad. Sci. USA *106*, 2194–2199.

Schaffer, B.E., Levin, R.S., Hertz, N.T., et al. (2015). Identification of AMPK phosphorylation sites reveals a network of proteins involved in cell invasion and facilitates large-scale substrate prediction. Cell Metab. *22*, 907–921.

Schirmer, E.C., Florens, L., Guan, T., et al. (2003). Nuclear membrane proteins with potential disease links found by subtractive proteomics. Science *301*, 1380–1382.

Schirmer, E.C., and Foisner, R. (2007). Proteins that associate with lamins: many faces, many functions. Exp. Cell Res. *313*, 2167–2179.

Schirmer, E.C., and Gerace, L. (2005). The nuclear membrane proteome: extending the envelope. Trends Biochem. Sci. *30*, 551–558.

Selvam, S., Kumar, T., and Fruttiger, M. (2018). Retinal vasculature development in health and disease. Prog. Retin. Eye Res. *63*, 1–19.

Shah, R.S., Soetikno, B.T., Lajko, M., et al. (2015). A mouse model for laser-induced choroidal neovascularization. J. Vis. Exp. *106*, e53502.

Stahl, A., Connor, K.M., Sapieha, P., et al. (2010). The mouse retina as an angiogenesis model. Invest. Ophthalmol. Vis. Sci. *51*, 2813–2826.

Staton, C.A., Reed, M.W., and Brown, N.J. (2009). A critical analysis of current in vitro and in vivo angiogenesis assays. Int. J. Exp. Pathol. *90*, 195–221.

Tobia, C., Gariano, G., Guerra, J., et al. (2015). Zebrafish embryo intersegmental vessels: a tool for investigating sprouting angiogenesis. Methods Mol. Biol. *1214*, 173–184.

Toma, H.S., Barnett, J.M., Penn, J.S., et al. (2010). Improved assessment of laser-induced choroidal neovascularization. Microvasc. Res. *80*, 295–302.

Tual-Chalot, S., Allinson, K.R., Fruttiger, M., et al. (2013). Whole mount immunofluorescent staining of the neonatal mouse retina to investigate angiogenesis in vivo. J. Vis. Exp. *77*, e50546.

Vijayaraghavan, B., Figueroa, R.A., Bergqvist, C., et al. (2018). RanGTPase regulates the interaction between the inner nuclear membrane proteins, Samp1 and Emerin. Biochim. Biophys. Acta Biomembr. *1860*, 1326–1334.

Zhou, H.J., Palma, S.D., Preisinger, C., et al. (2013). Toward a comprehensive characterization of a human cancer cell phosphoproteome. J. Proteome Res. *12*, 260–271.